論文 / 著書情報
Article / Book Information

Title	Retrospective earthquake spatial forecasting:magnetotelluric insights into fluid-driven intraplate seismicity in northern Thailand from 1994 to 2024
Authors	Puwis Amatyakul, Songkhun Boonchaisuk, Patchawee Nualkhao, Yasuo Ogawa, Weerachai Siripunvaraporn
Citation	Earth, Planets and Space, 77, ,
Pub. date	2025, 10
DOI	https://doi.org/10.1186/s40623-025-02301-x
Creative Commons	The information is in the article.

Earth, Planets and Space

FULL PAPER

Open Access

Retrospective earthquake spatial forecasting: magnetotelluric insights into fluid-driven intraplate seismicity in northern Thailand from 1994 to 2024

Puwis Amatyakul[1,2], Songkhun Boonchaisuk[3], Patchawee Nualkhao[3], Yasuo Ogawa[4,5] and Weerachai Siripunvaraporn[1,2*]

Abstract

This study investigates the role of crustal fluids in the seismogenesis of three significant intraplate earthquakes in northern Thailand: the 1994 Phan, 2014 Mae Lao, and the unexpected 2019 Wang Nuea events, which occurred after a decade of seismic quiescence. Utilizing 3D resistivity models derived from integrated 2015 and 2024 magnetotelluric (MT) surveys, we reveal complex, interconnected conductive systems beneath each seismically active region, indicative of fluid pathways extending from the lower to the near-surface crust. For the 2014 Mae Lao earthquake, a lower crustal fluid source ascends through a mid-crustal conductor with northward and southward extensions. A shared deep fluid source is implicated in the 1994 Phan earthquake; however, fluids follow a distinct southward migration pathway. The 2019 Wang Nuea earthquake also exhibits comparable lower and mid-crustal conductive structures and inferred fluid ascent, mirroring the Mae Lao system. Notably, a mid-crustal conductor was identified beneath the Wang Nuea region in our initial 2015 MT survey, but with the decades of seismic quiet, the link between this crustal fluid and the eventual earthquake was not anticipated, representing a missed opportunity for early spatial forecasting of the 2019 rupture. In all three events, the presence of fluids within the fault zones likely reduced their strength, leading to rupture when tectonic stress exceeded the critical threshold. The consistent presence of these conductive systems across these intraplate earthquakes suggests a unique characteristic of seismogenesis in northern Thailand, providing a valuable geophysical signature for future seismic hazard assessment and spatial forecasting.

Keywords Magnetotelluric, Northern Thailand, Fluid-driven seismicity, Intraplate earthquake, Spatial forecasting earthquake

*Correspondence:
Weerachai Siripunvaraporn
wsiripun@gmail.com
Full list of author information is available at the end of the article

Graphical Abstract

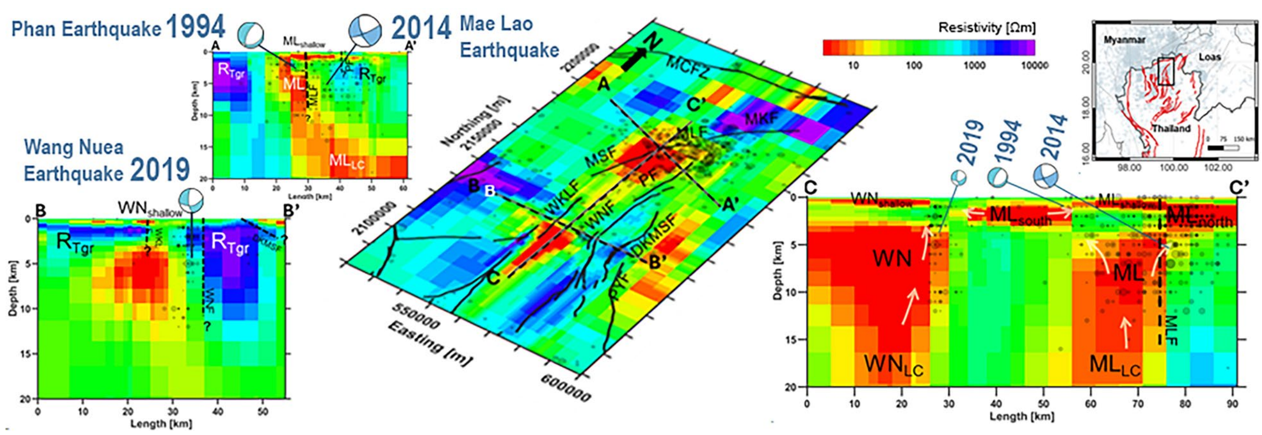

1 Introduction

Thailand is located within the Sunda Plate, formerly included as part of the Eurasian Plate but now recognized as a separate tectonic plate due to its distinct motion (Socquet et al. 2006). Its location is relatively far from the main collision zone, where the Indian Plate subducts beneath the Eurasian Plate. The effects of this distant Cenozoic collision are evident in the numerous faults present in northern Thailand (Fig. 1a). As a result, northern Thailand experiences relatively low intraplate seismicity (epicenters within Thailand), with earthquake magnitudes mostly below 3. Notably, earthquakes reaching magnitudes 4 and 5 have occurred infrequently over the past 50 years (less than 15 events), particularly when compared to its neighboring countries like Myanmar (Fig. 1a).

In the northernmost region of Thailand, the major left-lateral strike–slip Mae Chan Fault Zone (MCFZ) trends ENE–WSW, traversing northern Thailand from west to east and extending into the northeastern Laos (Fig. 1b). Despite being the longest fault in Thailand, seismicity along the MCFZ within Thailand has remained relatively quiet (Fig. 1a–d). However, geologists anticipate future slip along the MCFZ, which could generate large earthquakes in Thailand (Manopkawee et al. 2025). The high seismic potential of the MCFZ is evident from the Mw 6.3 earthquake that occurred on May 16, 2007, on a segment of the fault in northeastern Laos, with its epicenter approximately 270 km from Chiang Rai city, Thailand. Furthermore, the presence of numerous hot springs along the MCFZ in Thailand (Fig. 1b), such as Fang hot spring in the west (Amatyakul et al. 2023, 2016), and Mae Chan hot spring in the center (Amatyakul et al. 2023, 2021, 2015), indicates ongoing geothermal activity associated with this major fault system.

Over the past 30 years, most low-to-moderate magnitude earthquakes in northern Thailand have been concentrated along two major strike–slip fault zones (Fig. 1b): the ENE–WSW trending Mae Lao Fault Zone (MLFZ; blue in Fig. 1b) and the N–S trending Phayao Fault Zone (PYFZ; red in Fig. 1b). Prior to 2019, MLFZ was considered part of the PYFZ, as documented in several earlier publications (e.g., Noisagool et al. 2016; Boonchaisuk et al. 2017; Pananont et al. 2017; Tadapansawut et al. 2022). However, in 2019, the Department of Mineral Resources (DMR) of Thailand reclassified them as separate fault zones (DMR 2023).

The MLFZ (blue in Fig. 1b) comprises three major segments from north to south: the Mae Korn Fault (MKF), the Mae Lao Fault (MLF) and the Mae Suai Fault (MSF), respectively. While all were initially classified as left-lateral strike–slip faults (DMR 2023), the MSF was later reclassified as a west-dipping oblique-normal slip fault (Kanthiya et al. 2019). The PYFZ, with a total length of approximately 120 km, consists of numerous segments (red in Fig. 1b). Our work focuses mostly on the northern segments of the PYFZ (Fig. 1b). From north to south, these include the left-lateral strike–slip Phan Fault (PF) and the Wang Nuea Fault (WNF). Parallel to the WNF are the Wiang Kalong Fault (WKLF) to the west, and the Doi Khun Mae Suk Fault (DKMSF) and Phayao Fault (PYF) to the east. Although additional fault strands exist further south, our study area terminates near Wang Nuea district, and therefore, we exclude to mention them.

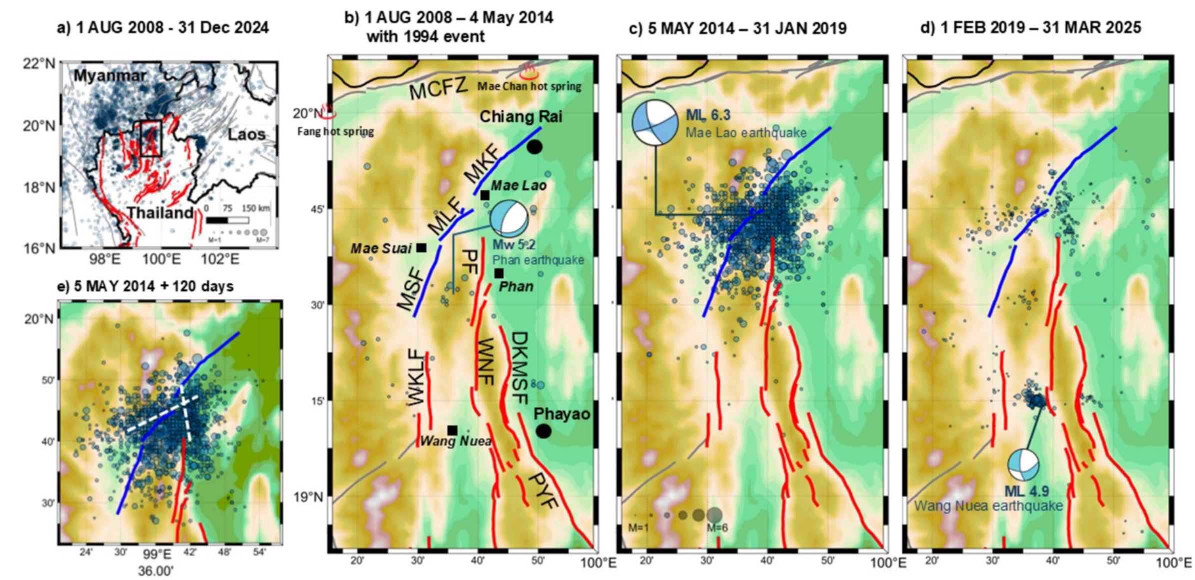

Fig. 1 **a** Northern Thailand and its neighboring countries, showing major fault traces (red solid lines) and seismicity (dark blue circles) from the Thailand Meteorological Department (TMD) from 1 Aug 2008 to 31 December 2024. The black rectangle indicates the location of the study. **b** Seismicity (blue circles) around the Mae Lao Fault Zone (MLFZ, blue) and the Phayao Fault Zone (PYFZ, red) prior to 5 May 2014 (from 1 August 2008 to 4 May 2014), including the Mw 5.2 Phan earthquake in 1994 with its focal mechanism (DMR 2019). Key fault zones labeled are: MCFZ (Mae Chan Fault Zone), for MLFZ: MKF (Mae Korn Fault), MLF (Mae Lao Fault), MSF (Mae Suai Fault), for PYFZ: PF (Phan Fault), WKLF (Wiang Kalong Fault), WNF (Wang Nuea Fault), DKMSF (Doi Khun Mae Suk Fault) and PYF (Phayao Fault). Locations of key cities (Chiang Rai and Phayao) and districts (Mae Lao, Phan, Mae Suai, and Wang Nuea) are also shown. **c** Seismicity from 5 May 2014 to 31 January 2019, showing the aftershock sequence of the Mw 6.3 Mae Lao earthquake of 5 May 2014, with its focal mechanism. **d** Seismicity from 1 February 2019 to 31 March 2025, showing the location of the Ml 4.9 Wang Nuea earthquake with its focal mechanism and aftershocks. **e** Two conjugated fault planes (white dashed lines) derived from relocated earthquakes during the initial 120 days following the Mae Lao earthquake (Pananont et al. 2017), plotted over the TMD seismicity

1.1 The 1994 Phan earthquake

Prior to the establishment of Thailand's modern seismic network, a moderate earthquake and its aftershocks strongly shook the Phan district, causing panic among residents and minor structural damages (Fig. 1b). The epicenter was located about 15 km southwest of the Phan district, close to the right-lateral strike–slip PF. The United States Geological Survey (USGS) estimated its local magnitude to be 5.2, with a focal mechanism indicating strike–slip faulting with a normal component (Fig. 1b). Subsequent focal mechanism analysis by Noisagool et al. (2016) suggested that this 1994 event could be reconstructed as a pure strike–slip motion, consistent with the characteristics of the PF. Since its epicenter was located close to the Phan district, we refer to this event as the Phan earthquake.

Beginning in 2008, modern seismometers have been increasingly installed throughout northern Thailand. We observe that the area, where the 1994 epicenter was located has actually been seismically active with small earthquakes (Fig. 1b) since 2008. Seismicity can also be observed in other time periods (Fig. 1c, d). Due to its proximity to the Phan Fault (PF), we will refer to this zone as the Phan seismic zone in the discussion section.

1.2 The 2014 Mae Lao earthquake

Nearly 20 years after the 1994 Phan earthquake, following a period of relative seismic quiet with only small magnitude earthquakes (Fig. 1b), the Mae Lao earthquake struck unexpectedly on May 5, 2014, and was felt in both the Phan and Mae Lao Districts in Chiang Rai province (Fig. 1c). The Thailand Meteorological Department (TMD) estimated its local magnitude at 6.3, making it the largest recorded earthquake in Thailand since the establishment of the seismometer network. This devastating earthquake caused damage to 594 buildings, exceeding that of any other seismic events in the country's history, and resulted in one casualty and hundreds of injuries (Lukkunaprasit et al. 2015). The epicenter of the mainshock and subsequent aftershocks, as located by TMD, were primarily distributed within the transition zone between the MLFZ and PYFZ (Fig. 1c). The mainshock hypocenter, located closer to the MLF (Fig. 1c), was at a depth of around 6 km. Due to its proximity to the Mae

Lao District (Fig. 1c), this event was subsequently named as the Mae Lao earthquake.

Note that while preparing for this paper, a powerful earthquake with a magnitude of Mw 7.7 struck Mandalay, Myanmar on March 28, 2025, with its epicenter located on the Sagaing Fault, a fault considered among the most tectonically active within the Sunda Plate region, as evidence by the frequent occurrence of large magnitude earthquakes (Tsutsumi et al. 2009). Although the distance from the epicenter is approximately 400–500 km from the northern major cities of Thailand, and 1000 km from the capital Bangkok, its effect was devastating, causing more life loss and damage than any other events in Thailand's seismicity history, including the Mae Lao earthquake. However, the epicenter of this Myanmar earthquake was outside of Thailand, while the epicenter of the Mae Lao earthquake was within Thailand.

Using data from the recent regional seismometer network, Noisagool et al. (2016) derived 30 focal mechanisms from the main event and aftershocks. They found that 24 of them exhibited strike–slip with normal motion, four showed strike–slip with thrust motion, and two were reversed faulting. The hypocenter of the main event was estimated at around 11 km depths, slightly deeper than initially estimated by TMD, with a moment magnitude (Mw) of 6.5. Based on stress inversion from these 30 focal mechanisms, Noisagool et al. (2016) determined that the principal stress originated from the N18°E direction. Furthermore, by plotting the fault plane solutions on a Mohr's circle diagram, they observed that the ENE–WSW trending MLF exhibits greater instability under the N18°E regional stress compared to other faults of Thailand, particularly the nearly W–E trending MCFZ in the north and the N–S trending PF in the south (Fig. 1b). They concluded that the accumulation of regional stress from the north eventually exceeded the fault strength threshold, causing the MLF to slip first and generate the 6.5 Mw mainshock on May 5, 2014. The seismic wave energy then propagated and transferred to other segments of both MLFZ and PYFZ, producing many aftershocks with mixed mechanisms throughout the transition zone.

In a separate study, Pananont et al. (2017) used the double-difference algorithm to relocate the epicenters of the mainshock and aftershocks. They found that the mainshock epicenter estimated by TMD should be slightly shifted southward to an area north of the Phan Fault (PF) with a hypocenter centroid depth of 12 km. They also found that most focal mechanisms of both mainshock and aftershocks showed strike–slip motion along two nodal conjugate planes: a right-lateral NNW-trending plane and left-lateral ENE trending plane (Fig. 1e). Based on stress modeling, they inferred that the mainshock likely initiated along the right lateral north–south trending Phan Fault (PF) before propagating to the left lateral conjugate MLF for the aftershocks.

Tadapansawut et al. (2022) applied the potency density tensor inversion method to the 2014 events and concluded that the 2014 rupture consisted of two distinct episodes occurring on both conjugated strike–slip faults as of Pananont et al. (2017) shown in Fig. 1e. The first rupture episode of the mainshock (0–2 s) initiated at the hypocenter and propagated southward along the N–S trending fault plane, terminating just north of the PF. The second episode (2–4.5 s) began north of the epicenter at the edge of the E–W trending fault plane and propagate southwestward. All these studies (Noisagool et al. 2016; Pananont et al. 2017; Tadapanswut et al. 2022) indicated that the rupture process of the 2014 events exhibited complex characteristics.

1.3 The 2019 Wang Nuea earthquake

Although aftershocks from the 2014 Mae Lao earthquake have continued to the present day, the region around the PYFZ, south of the transition zone between MLF and PF, had remained quiet for an extended period (Fig. 1c). On the morning of February 20, 2019, surprisingly, following several small foreshocks, a 4.9 local magnitude earthquake struck the Wang Nuea region (Fig. 1d), triggering hundreds of small aftershocks. This 4.9 magnitude earthquake was unusually large for this nearly aseismic zone, causing panic among residents and resulting in minor damage to over 80 houses and buildings in the area.

According to TMD, its main shock epicenter was located near the Wang Nuea Fault (WNF; Fig. 1d), approximately 60 km south of the 2014 Mae Lao earthquake epicenter (Fig. 1c). The focal mechanism indicated strike–slip faulting (Fig. 1d). To date, there are no published research studies on this Wang Nuea earthquake, possibly because most of the events were small-magnitude earthquakes (< M4). As its epicenter is located north of the Wang Nuea district, this 2019 earthquake is then referred to as the Wang Nuea earthquakes. While seismic activity continued beyond 2019, its frequency decreased significantly over time (Fig. 1d).

1.4 The fluid-driven mechanism for the 2014 Mae Lao earthquake

With the advent of practical and accessible 3D MT inversion techniques, the magnetotelluric (MT) method, a passive electromagnetic technique, has been increasingly used worldwide to investigate the relationship between resistivity structure around fault zones and earthquake occurrence regions, particularly since the 2010s. Frequently, fluids within conductive anomalies in the upper crust play critical roles in fault zones, triggering the earthquakes in the region (Li et al. 2019, 2021; Zhang et al. 2024; Zhou et al. 2025; Aizawa et al. 2017; Aizawa et al. 2021; Boonchaisuk et al. 2017, 2013; Becken and Ritter 2012; Cheng et al. 2022; Ichihara et al. 2023; Egbert et al. 2022; Borah et al. 2023; Kothyari et al. 2023; Usui et al. 2021, 2024; Cai et al. 2017; Kang et al. 2023; Ogawa et al. 2001, 2002, 2014; Kumar et al. 2017; Tank et al. 2005; Kaya et al. 2013).

In November 2015, approximately 1.5 years after the 2014 Mae Lao earthquake, we deployed 31 MT stations across a 140 km × 140 km survey area to investigate the subsurface resistivity structure and its relationship to the 2014 Mae Lao earthquake (Fig. 2; Boonchaisuk et al. 2017). In the northern part of this area, these stations were distributed to cover all segments of the MLFZ, as well as the Phan Fault (PF), with a greater number of stations perpendicular to the MLF fault strike, focusing on the MLF–PF transition zone. Following data processing and 3D inversion, Boonchaisuk et al. (2017) obtained a final 3D resistivity model with calculated responses closely matching the acquired data and near surface resistivity consistent with the regional geology. This 2015 model revealed several notable anomalies from the near surface to greater depth (Fig. 2; Boonchaisuk et al. 2017).

One particularly interesting conductive anomaly (designated as ML in Boonchaisuk et al. 2017; Fig. 2) was found extending from a depth of 5 km to mid-crustal depth (Fig. 2a–c). This ML anomaly is located primarily beneath the MLF (Fig. 2a–c), coinciding with the mainshock hypocenter and aftershocks of the 2014 Mae Lao earthquake. We interpreted this ML conductor as a saline fluid-rich zone (Boonchaisuk et al. 2017). As tectonic stress continued to accumulate from the north (Noisagool et al. 2016), it increased the pore pressure within the fluid, therefore, reducing the frictional strength along the MLF. When the accumulated tectonic stress exceeded a critical threshold, it triggered a slip along the MLF (Boonchaisuk et al. 2017), resulting in the largest earthquake in Thailand's recorded history on 5 May 2014 and thousands of aftershocks.

1.5 Missed opportunity for earthquake spatial forecasting for the 2019 Wang Nuea earthquake

Despite the relatively quiet seismicity in the area south of the MLF–PF transition zone, both during and after the Mae Lao earthquake (Fig. 1b, c), two MT profiles of the 2015 MT survey were deployed extending southward from this transition zone to cover all the northern segments of the PYFZ, terminating near Wang Nuea district (Fig. 2). Both MT profiles were oriented almost perpendicular to the strikes of the WKLF, and WNF (Fig. 2; Boonchaisuk et al. 2017).

Based on the final resistivity model of the 2015 MT survey (Fig. 2; Boonchaisuk et al. 2017), it was intriguing to observe another large conductive anomaly at depths of 4–15 km between the two WKLF and WNF segments of the PYFZ (Fig. 2a–d), near the Wang Nuea district and approximately 60 km directly south of the ML conductor (Boonchaisuk et al. 2017). It was initially designated as the P2 conductor in Boonchaisuk et al. (2017); however, due to its proximity to the Wang Nuea district, we have renamed it here as the WN conductor.

Although this WN conductor shared similarities with the ML conductor beneath the MLF, with limited MT stations, the absence of seismic activity in the region through 2015 (Fig. 1b, c) led us to initially dismiss any

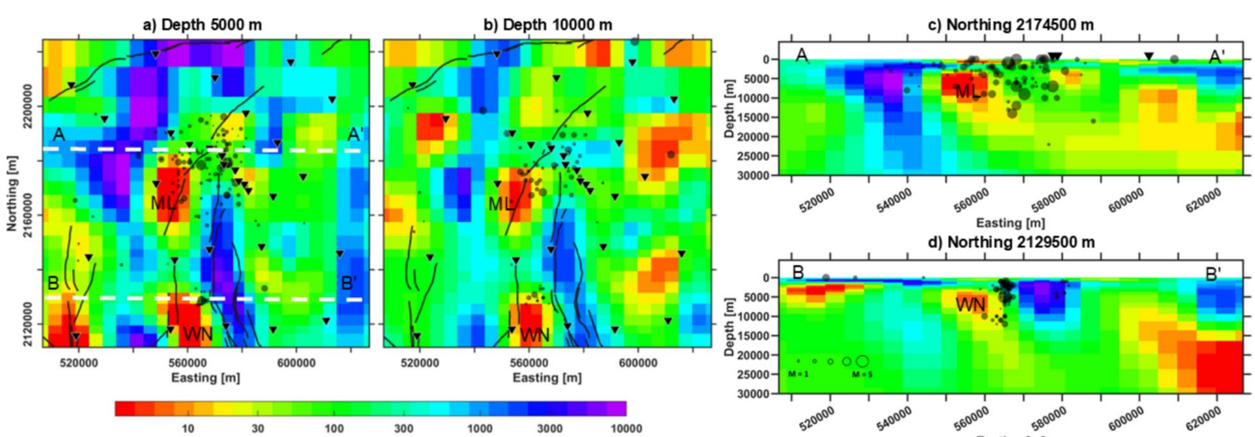

Fig. 2 Top view of the resistivity model derived from the 2015 MT survey (Boonchaisuk et al. 2017) at depths of **a** 5 km and **b** 10 km, overlain with seismicity from the TMD. Cross-sectional profiles of the resistivity model along lines A–A′ and B–B′ are shown in (**c, d**), respectively, also displaying TMD seismicity. The color bar represents the resistivity in Ω m. Black triangles indicate the locations of 2015 MT stations, and solid black lines are fault traces as in Fig. 1b

potential connection to future earthquakes. In addition, because the WN conductor was located near the edge of the survey area, where MT station density was sparse (Fig. 2a, b), we were not certain about its size and depth of the conductor. Our preliminary interpretation at that time (Boonchaisuk et al. 2017) attributed it to a local hot spring source nearby, similar to other hot spring sources in other regions of the northern Thailand (Amatyakul et al. 2015, 2016, 2021, 2023).

Surprisingly, in February of 2019, a 4.9 local magnitude earthquake shook the Wang Nuea district (Fig. 1d) with hundreds of aftershocks. Even more surprising in relation to our previous 2015 MT survey (Boonchaisuk et al. 2017), the 2019 epicenters were primarily clustered between the WNF and WKLF (Fig. 2a, b, d), coincidingly with our identified WN conductor. If we had interpreted this WN conductor as a fluid-rich zone with a similar rupture mechanism to the ML conductor, we might have been able to forecast the location of future earthquake occurrences, though not their timing. This represents a missed opportunity for earthquake spatial forecasting but also provides a valuable lesson learned.

1.6 Objectives of our research

To confirm the existence of the WN conductor and to understand whether the rupture mechanism of the 2019 Wang Nuea earthquake is fluid-driven, similar to the 2014 Mae Lao earthquake, we conducted an additional MT survey in 2024. This survey targeted the region above the Wang Nuea earthquake zone, addressing the inadequate MT station coverage from the 2015 survey. The 2024 survey not only focused on the Wang Nuea region but also extended southward to image the subsurface resistivity structure across the northern segments of the PYFZ beyond the Wang Nuea district.

The newly acquired data from the 2024 survey were then integrated with the 2015 survey data. The combined data set from both surveys was reprocessed, and a 3D inversion was performed to better constrain the resistivity structures, clearly revealing the ML and WN conductors, other key anomalies, and a well-defined delineation of the brittle–ductile transition (BDT) zone based on the resistivity gradient with depth. The resulting resistivity structure will be reinterpreted and reevaluated, incorporating recent earthquake seismology, geological and geophysical findings (Noisagool et al. 2016; Pananont et al. 2017; Tadapanswut et al. 2022; and others) to explain the rupture mechanisms of both the 2014 Mae Lao earthquakes and the 2019 Wang Nuea earthquakes, which could mark a characteristic of intraplate earthquakes in northern Thailand. In addition, we will also use knowledge learned from both areas to revisit the 1994 Phan earthquakes, and to explore the possibility of spatial forecasting of future earthquake locations within this intraplate setting.

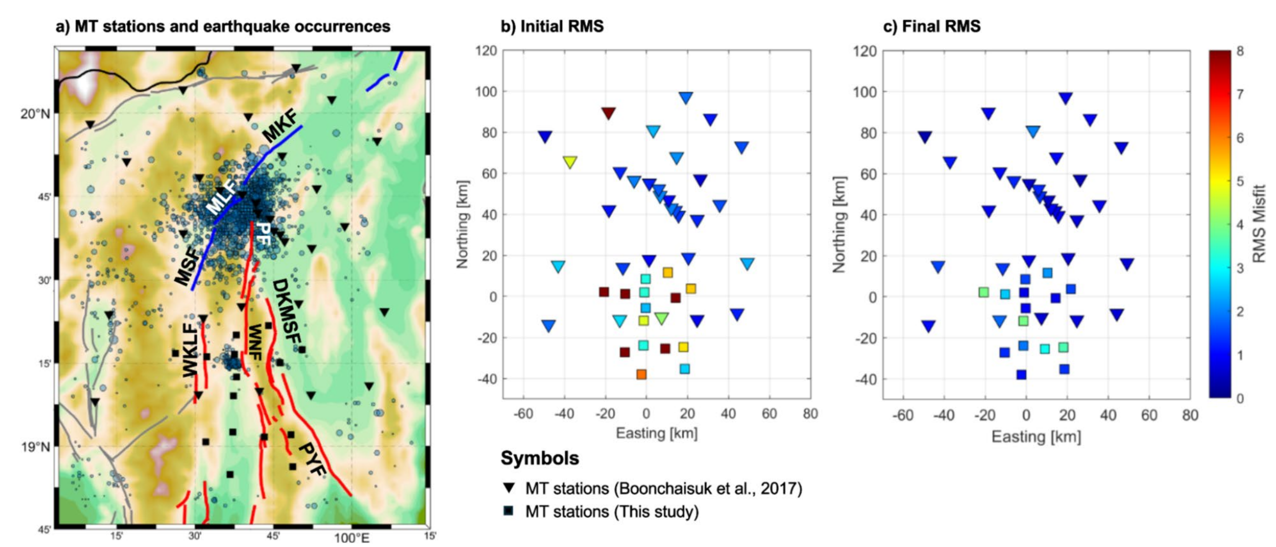

Fig. 3 **a** Map showing the locations of MT stations deployed around the MLFZ (blue lines) and the PYFZ (red lines) with earthquake epicenters (blue circles) from the TMD. Inverted black triangles represent stations from the 2015 survey (Boonchaisuk et al. 2017), while black squares indicate stations from the 2024 survey conducted in this study. The distribution of the RMS misfit for each MT station (**a**) during the initial inversion run with a total RMS for all stations of 5.8, and (**c**) after the 3rd iteration with a reduced total RMS for all stations of 1.58

2 The 2024 MT survey, data processing and the 3D MT inversion

Following the 2019 Wang Nuea earthquake, we initiated additional MT site deployments around the Wang Nuea region in 2020 to confirm the WN conductor identified in the earlier 2015 MT survey (Fig. 2; triangles in Fig. 3a; Boonchaisuk et al. 2017). However, this 2020 survey was canceled due to the COVID-19 pandemic, which restricted access to the survey area. The survey plan was revised and implemented in 2024, resulting in the deployment of 19 MT stations. Unfortunately, four of these stations yielded poor-quality data and were excluded, leaving 15 new stations for this study (squares in Fig. 3a). To address the sparse MT station coverage directly above the WN conductor (Fig. 2), we strategically deployed eight additional MT stations (squares in Fig. 3a) over and adjacent to this conductor. This targeted deployment aimed to cover the epicenters of the Wang Nuea earthquake zone, located between the two southern MT profiles acquired in 2015. Furthermore, to constrain the southern extent of the WN conductor beyond the Wang Nuea district, seven more MT stations (squares in Fig. 3a) were installed south of the 2015 MT survey area boundary.

Our 2024 MT survey employed the same acquisition methodology as the 2015 survey (Boonchaisuk et al. 2017). Specifically, a set of KMS Technologies MT systems was deployed to record the horizontal electric and magnetic fields at various sampling frequencies. Due to a limited number of coils, the vertical magnetic field was not recorded during this survey. The equipment was typically left overnight and relocated to a new site the following morning. Another set of MT systems was set up at a remote reference site, about 500 km south of the survey area in Kanchanaburi province, to enhance data quality. The data acquired at the Wang Nuea sites, along with the remote reference site, were simultaneously processed using KMS software and the robust remote reference technique (Egbert 1997) for the impedance tensor **Z**. Despite some sites appearing naturally quiet, the data proved to be electrically noisy for an undetermined reason and could not be adequately cleaned, even with the remote reference technique. These data sites were then excluded, leaving at a total of 15 stations with good and acceptable data quality.

The data from the 15 new stations (squares in Fig. 3a) were then merged with the 31 stations (triangles in Fig. 3a) from the 2015 acquisition, resulting in a total of 46 stations. As the sampling frequencies used in the 2024 survey differed slightly from those in the 2015 survey, we reprocessed the 2015 survey data to ensure a consistent frequency range and further enhance data quality. Following reprocessing, we obtained 16 periods of good and acceptable off-diagonal impedance tensors (Z_{xy} and Z_{yx}) ranging from 320 Hz to about 320 s for each site, while the diagonal impedance (Z_{xx} and Z_{yy}) was highly contaminated and were excluded for the 3D MT inversion. The Z_{xy} and Z_{yx} impedance tensor components from these 46 sites were then inverted using the parallel version of WSINV3DMT (Siripunvaraporn et al. 2005; Siripunvaraporn and Egbert 2009; Siripunvaraporn and Sarakorn 2011; Thongyoy et al. 2025) to generate the 3D resistivity model. The minimum error floors were set at 5%. For the 3D inversion of these 46 stations, we used the final inverted resistivity model from our previous 2015 acquisition (Boonchaisuk et al. 2017) as both the initial and background model. This prior model was chosen, because its calculated responses closely matched the acquired 2015 data, and its near-surface resistivity was consistent with the regional geology.

With the addition of 15 new sites, the grid discretization of 52×52×44 (with 7-air layers on top of the topography) in the north–south, west–east and vertical directions, respectively, used in the final model from the 2015 acquisition (Boonchaisuk et al. 2017) was no longer sufficient to accurately represent these new sites. Therefore, a new grid discretization of 60×70×42, with an additional 7 air layers, was created. The horizontal discretization of the modeling grid varied to optimize resolution based on station density. Cells within the densest MT station areas were refined to 1–2 km×1–2 km. For most other sites, a discretization of 2–3 km×2–3 km was used. At the outermost stations, the grid cells expanded to 3–5 km×3–5 km. This variable cell sizing ensured high accuracy, where station coverage was dense while maintaining computational efficiency across the broader model domain. The horizontal grid discretization included grid spacing that increased logarithmically outside the study area to avoid the boundary effects (Siripunvaraporn et al. 2002; Siripunvaraporn 2012). The final model of Boonchaisuk et al. (2017) was then merged and interpolated onto this newly created grid and subsequently used as the initial model and background model for the 3D inversion.

Using the final model from the 2015 survey (Boonchaisuk et al. 2017) as the initial model for inversion, the initial RMS misfit was about 5.8. As expected, given that this initial model was optimized solely for the 2015 data, all 15 newly acquired stations exhibited higher RMS misfit (squares in Fig. 3b), while most of the 2015 MT stations showed lower RMS misfits (triangles in Fig. 3b). However, a few of the 2015 stations displayed higher RMS misfits than those reported in Boonchaisuk et al. (2017), which resulted from improved data quality after reprocessing. Following three iterations of the WSINV3DMT inversion, the overall RMS misfit decreased

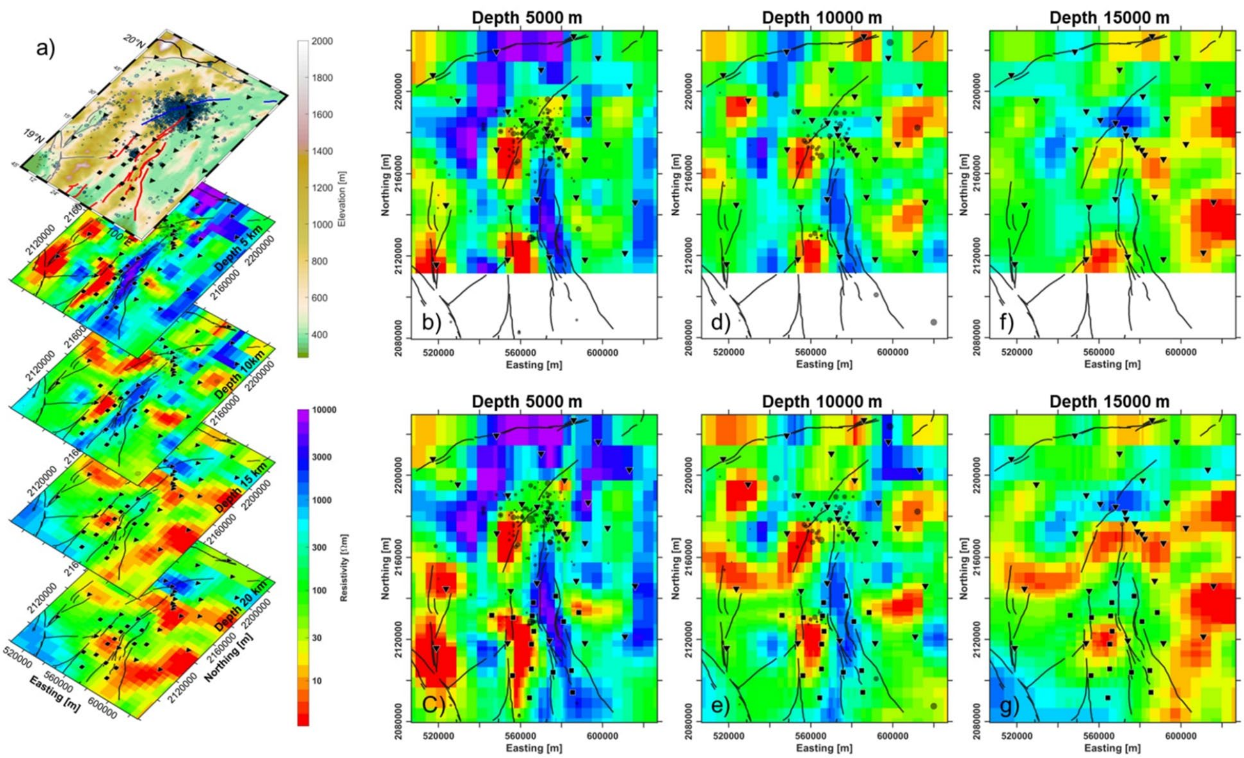

Fig. 4 a Final 3D resistivity model derived from the combined 2015 and 2024 MT survey. Comparison of the resistivity models at selected depths from **b, d, f** 2015 MT survey (top row) and **c, e, g** combined 2015 and 2024 MT survey (bottom row)

significantly to 1.5 (Fig. 3c), and this final RMS included the majority of the reprocessed 2015 stations. The resulting resistivity model from the third iteration is presented in Fig. 4a.

Given that we used the final 2015 resistivity model from Boonchaisuk et al. (2017) as our starting model for this inversion, a similarity in the underlying structures between our final 2015 (Fig. 2) and 2024 (Fig. 4a) resistivity models is expected, particularly in the consistency of the locations of the major conductive (red to orange in Fig. 4b, c) and resistive (blue in Fig. 4b, c) anomalies at corresponding depths. However, the expanded 2024 survey area (Fig. 4c), extending further southward than the 2015 survey (Fig. 4b), provides a better and broader understanding of the subsurface resistivity structure near the Wang Nuea seismic zone. For instance, the prominent conductive anomalies near the Wang Nuea zone (Fig. 4c) associated with the PYFZ in the south of the survey area appear more continuous and focused in the 2024 model. Furthermore, the integrated data set (Fig. 4c) yields significant enhancements in resolution and detail, characterized by sharper boundaries between resistivity contrasts and the increased resolution of finer-scale structures at all depths, as exemplified by the increased sharper boundaries of the resistive zone near the Phan seismic zone in the 2024 model (Fig. 4c).

A major interesting observation in the 2024 model (Fig. 4c) is the appearance of broader conductive anomalies at greater depths, exhibiting continuity and interconnection with fewer resistive features, a behavior less apparent in the more scattered conductive anomalies of the 2015 model (Fig. 4b). This enhanced resistivity structure allows for a more robust interpretation, particularly regarding the relationship between the conductive anomalies and fluids, the fault systems, and the corresponding seismicity in the region. Note that the robustness of all interpreted structures has been verified through sensitivity analysis, using the same technique previously employed in Boonchaisuk et al. (2017). This involved replacing target anomalies with background resistivity and observing the resultant increase in data misfit, confirming their necessity to fit the observed data.

3 Regional geology and tectonic evolution

Our MT survey area around the MLF and PYFZ in northern Thailand has experienced a complex tectonic evolution spanning from the Proterozoic to the Quaternary, evidenced by the diverse geological units exposed at

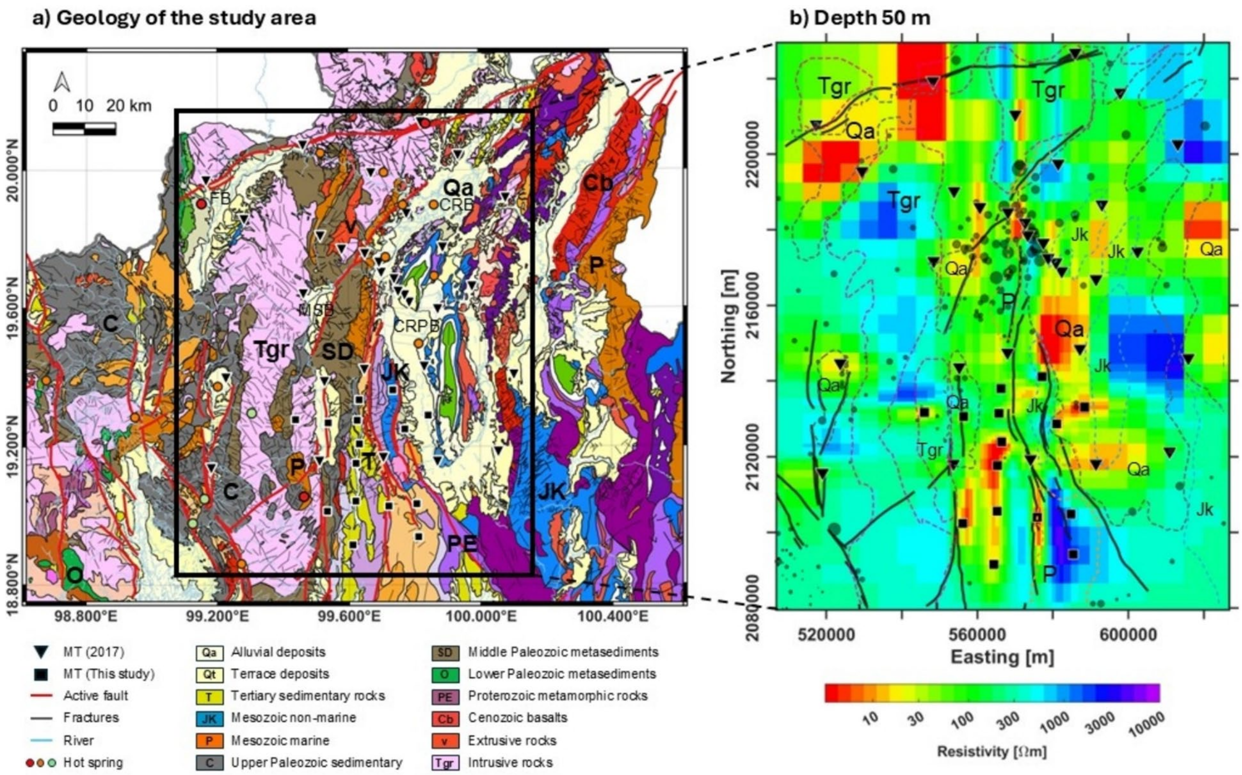

Fig. 5 **a** Geological map of the study area, showing various lithological units and major active faults (red lines), fractures (thin black lines), hot springs (red, orange and green circles), and locations of MT stations from the 2015 survey (inverted black triangles) and the 2024 survey (black squares). Selected basin are: FB (Fang Basin), MSB (Mae Suai Basin), CRB (Chiang Rai Basin) and CRPB (Chiang Rai–Phayao Basin). **b** Resistivity depth slice at 50 m below the surface, extracted from the final 3D inverted model (Fig. 4a)

the surface (Fig. 5a). In the southwestern region (Fig. 5a), Proterozoic metamorphic rocks (PE) are found, indicating a collisional event during the Permian and Triassic (Metcalfe 1997, 2013). The central fold belt, which covers the majority of the study area, developed as a magmatic arc along the margin of the eastern terrane during the Permian and Triassic periods (Sone and Metcalfe 2008; Sone et al. 2012). This belt is characterized by a mix of elongated sedimentary sequences, including Paleozoic (SD, C in Fig. 5a) and Mesozoic (P, Jk in Fig. 5a) sedimentary rocks, with volcanic rocks scattered throughout. These rocks are overlain and intruded by extensive Triassic granites (Tgr in Fig. 5a; Charusiri et al. 1993), which are exposed throughout the western and central zones of the study area (black rectangle in Fig. 5a) and are also found scattered in the eastern region of the fault zones.

During the Cenozoic, the collision of the Indian and Eurasian plates led to significant folding and strike–slip faulting (Uttamo et al. 2003), clearly visible at the surface as the Mae Lao Fault Zone (MLFZ) and the Phayao Fault Zone (PYFZ), the primary focus of this study (Fig. 5a). This collision also resulted in the formation of extensional and pull-apart basins in northern Thailand (Charusiri and Pum-Im 2009; Morley et al. 2011). The rifting associated with this process created numerous north–south trending basins, now filled with Tertiary sedimentary rocks (T in Fig. 5a) and Quaternary alluvial and terrace deposits (Qa; Qt in Fig. 5a). The presence of extrusive rocks and Cenozoic basalts (Cb) along fault zones indicates past volcanic activity, although the area currently exhibits no active volcanism. The multiple hot springs (Fang, Ban Nong Krog, Huai Sai Khao, and Sob Pong) observed along fault zones are primarily attributed to deep circulation of groundwater heated by the granite batholiths (Tgr in Fig. 5a), with the faults acting as conduits for the heated water to reach the surface (Amatyakul et al. 2023, 2021, 2016, 2015).

3.1 Matching the near-surface resistivity model with surface geology with

The final resistivity model in Boonchaisuk et al. (2017) was selected based on two criteria: a low RMS misfit and a close match between the near-surface resistivity model and the surface geology. Similar to Boonchaisuk et al. (2017), these two criteria were applied in this study for the selection of the final resistivity model shown in Fig. 4a. As demonstrated in Fig. 3b, this final resistivity model (Fig. 4a) yields a low RMS misfit. Here, we will show that the near-surface resistivity (Fig. 5b) is consistent with the surface geology (Fig. 5a).

The near-surface resistivity model (Fig. 5b) reveals distinct zones of resistive and conductive bodies. The resistive bodies (> 300 Ω m; Fig. 5b) correlate well with the Triassic granite rock (Tgr; Fig. 5a) in the western part of the study area. In addition, intermediate to high resistivity values are observed corresponding to the Mesozoic non-marine sediments (Jk; Fig. 5a), which are scattered around the alluvial deposit in the eastern part. Conversely, the lower resistive bodies (< 100 Ω m; Fig. 5b) mostly correspond to the Quaternary alluvial deposit (Qa; Fig. 5b; Morley et al. 2011), such as those in the Fang Basin (FB in Fig. 5a) in the northern part of the study area, the Mae Suai Basin (MSB in Fig. 5a; Kanthiya et al. 2019) next to the MSF, and the Chiang Rai Basin (CRB in Fig. 5a) and Chiang Rai–Phayao Basin (CRPB in Fig. 5a) east of the PYFZ. The moderate resistive bodies (100–300 Ω m; Fig. 5b) are primarily located within the PYFZ between the WNF and WKLF, corresponding to the Silurian/Devonian meta-sediments (SD; Fig. 5b) and volcanic rocks. The consistency between the surface geology and our near-surface resistivity model led us to select this model (Fig. 4a) as the final model for interpretation and discussion in the following section.

4 Interpretation and seismotectonic implications

Our resistivity model, derived from both the 2015 and 2024 MT surveys (Figs. 6, 7), reveal a complex three distinct resistivity layer structure beneath the PYFZ and MLFZ study area, offering critical new insights into the heterogeneous seismotectonic setting of the northern Thailand region and the potential influence of crustal fluids.

4.1 *Shallower heterogeneous layer (surface to ~ 4 km)*

The uppermost 4 km exhibits significant lateral and vertical variations in electrical resistivity directly reflecting the complex near-surface geology (Fig. 6a), as illustrated in the resistivity slices at 500 m (Fig. 6b) and 2000 m (Fig. 6c), and in all vertical cross sections of Fig. 7a–c.

The presence of highly resistive zones throughout the western flank of the major fault zones at these depths (R_{Tgr}; Fig. 6b, c), in conjunction with the tectonic setting and geology of the region (Fig. 6a), strongly suggests that these western resistive zones indicate outcropping Triassic granite intrusion at the surface (Tgr; Figs. 3, 6a), which can also be seen extending to greater depths in cross sections, Fig. 7a, b. In contrast, on the eastern flank of the fault zones, the tectonic setting differs slightly. Limited surface exposure of granite and a larger volume of overlying Mesozoic non-marine sediments (Jk, Figs. 3, 6a) implies that the granite batholith may only partially reach the surface, displacing the Mesozoic sediments

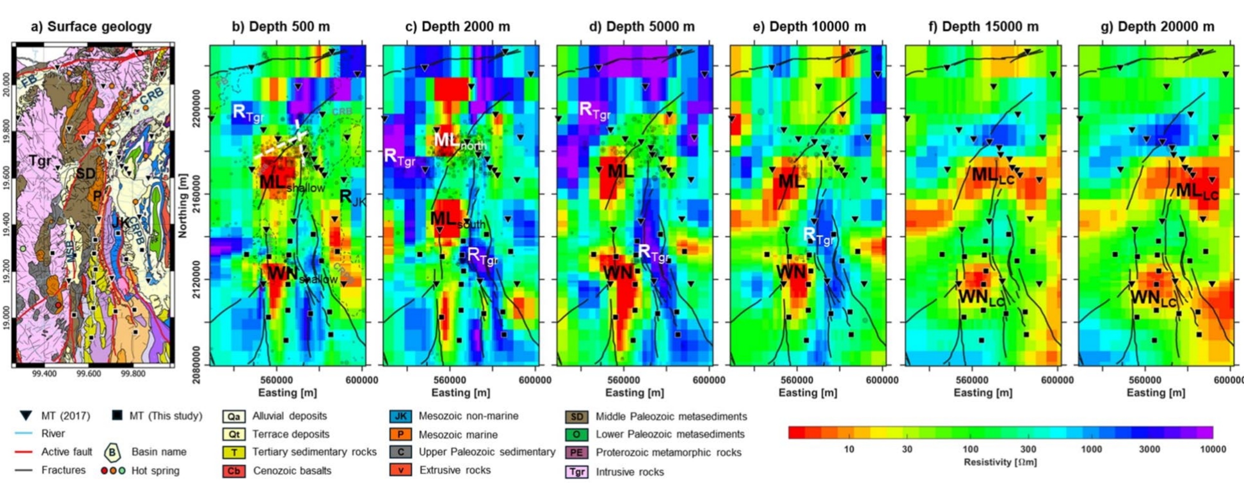

Fig. 6 **a** Surface geological map of the study area (extracted from Fig. 5a). **b–g** Top-view resistivity maps at depths of: **b** 500 m, **c** 2 km, **d** 5 km, **e** 10 km, **f** 15 km, and **g** 20 km below the surface. Overlaid on the resistivity maps are TMD epicenters (grey circles), major faults (thin black lines), MT stations (triangles and squares), relocated fault planes (white lines in (**b**); Pananont et al. 2017), and labeled conductive anomalies ($ML_{shallow}$, ML_{north}, ML_{south}, ML, ML_{LC}, $WN_{shallow}$, WN, and WN_{LC}) and resistive Triassic granite (R_{Tgr}) and resistive Mesozoic non-marine sediments (R_{jk})

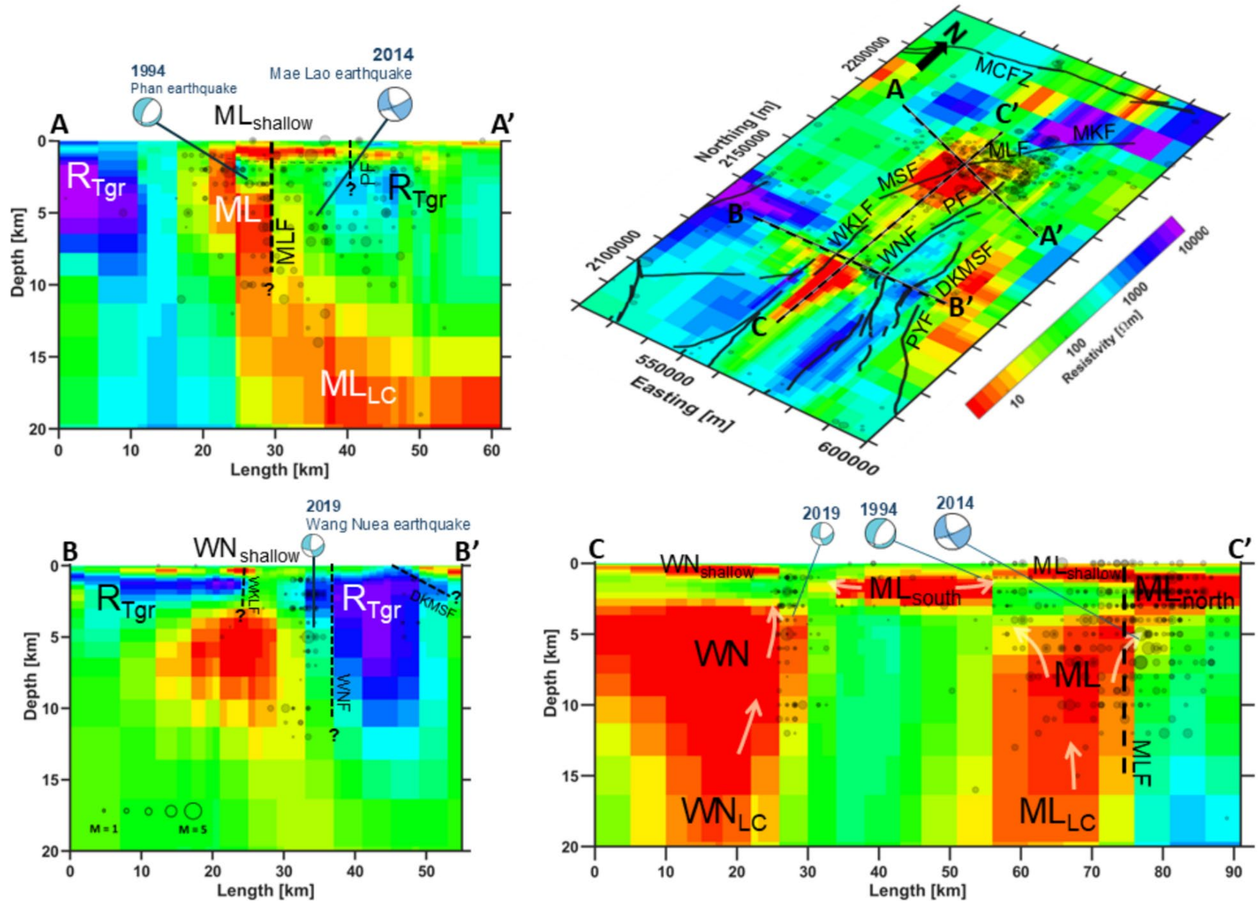

Fig. 7 Three vertical resistivity cross sections extracted from the 3D resistivity model (Figs. 4a, 6): **a** A–A′ cutting through the MLF, the MLF–PF transition zone, and the PF; **b** B–B′ cutting through the WKLF and WNF; and **c** C–C′ running from north to south, cutting through the MLF and parallel to the WNF. Projected earthquake hypocenters within a ± 2 km bin and the focal mechanisms of the 1994 Phan earthquake, 2014 Mae Lao earthquake, and 2019 Wang Nuea earthquake are also shown on these cross sections

upwards. This interpretation is supported by moderate to high resistive zones at 500 m depth (R_{Jk}; Fig. 6b), corresponding to the non-marine sediments (Jk, Fig. 6a), and the resistive zones at 2000 m depth (R_{Tgr}; Fig. 6c), associated with the granite intrusion (T_{gr}), which appear to extend to greater depths in cross sections A–A′ (Fig. 7a), and B–B′ (Fig. 7b).

Conversely, prominent conductive zones ($ML_{shallow}$, $WN_{shallow}$; Fig. 6b) are localized within the fault zones (MLF, PYFZ) in the shallower part of this upper layer, and are clearly evident near the surface extending to depths of a few kilometers in cross sections A–A' (Fig. 7a), and C–C' (Fig. 7c) for $ML_{shallow}$, and B–B' (Fig. 7b) and C–C' (Fig. 7c) for $WN_{shallow}$. Although the locations of these conductors are spatially associated with the sedimentary basins (Fig. 6a), it is unlikely that these low resistivity values (< 10 Ω-m) are solely attributed to sedimentary rocks, fractured granite, or a combination of both structures. Given the potential of fluid entrapment within these zones due to higher porosity, we interpret these shallow conductive zones as indicating the presence of saline fluids within the fractured granite and sediments surrounding the fault zones.

It is particularly interesting to observe that most hypocenters of the 2014 Mae Lao earthquakes are situated in the vicinity of or within the $ML_{shallow}$ conductor in the cross-sectional views (A–A', and C–C' in Fig. 7a, c). Furthermore, the top-view plot (Fig. 6b) reveals that the relocated hypocenter fault planes of the 2014 Mae Lao earthquakes (white lines in Fig. 6b; Pananont et al. 2017) encompass the northwestern edges of the $ML_{shallow}$ conductor. Similarly, the hypocenters of the 2019 Wang Nuea earthquake are also located near the edges of these shallow $WN_{shallow}$ conductive anomalies (Fig. 6b; B–B' in Fig. 7b). This close spatial relationship strongly suggests a significant link between fluid presence and seismic activity.

With increasing depth within this shallower heterogeneous layer (Fig. 6c), the $ML_{shallow}$ conductor, situated between the MLF–PF transition zone, appears to split into two distinct and deeper conductive zones: a northern zone (ML_{north}) located to the north and a southern zone (ML_{south}) located to the south (Fig. 6c; and C–C' in Fig. 7c). Interestingly, the northern conductor (ML_{north}) partially overlaps with the Mae Lao seismicity from TMD (Fig. 6c) and is located mostly north of the conjugated fault planes from the relocated earthquakes (Pananont et al. 2017). In contrast, the southern conductor (ML_{south}) appears to be situated within a seismic gap between the Mae Lao and Wang Nuea seismic regions to the north and south, respectively (Fig. 6c). Both ML_{north} and ML_{south} conductors are interpreted as fluid-rich zones within fractured granite and could potentially act as storage zones for fluids ascending from deeper levels (C–C' in Fig. 7c).

4.2 *Mid-crustal resistive layer and localized fluid accumulations (~ 4–15 km)*

The mid-crustal resistivity layer is characterized by a generally dominant high resistivity host extending from about 4 to 15 km depths, likely to represent the extensive granite batholiths (RT_{gr}; Figs. 6d, e, 7a, b). Within this resistive background, two distinct and localized conductive anomalies (ML, and WN in Fig. 6d, e) persist within or adjacent to the fault zones and also extend to greater depth even beyond the l5 km boundary, as clearly observed in the cross sections of Fig. 7 (ML in A–A' and C–C', and WN in B–B' and C–C'). The low resistivity values (< 10 Ω m) within these three mid-crustal conductors strongly suggest the presence of interconnected saline fluids. Based on the tectonic setting of the region, the origin of these accumulated fluids, manifesting as these conductive anomalies (ML, and WN), can be either derived from deeper crustal sources, migrating upwards along fault pathways and becoming trapped in fractured zones within the resistive granite, or alternatively, they might represent fluids expelled from deeper sedimentary sequences during tectonic compression and Triassic granite intrusion, or a combination of both.

It is interesting to observe a distinct correlation between the locations of these ML and WN anomalies and the hypocentral locations of the Mae Lao and Wang Nuea earthquakes (Figs. 6d, e, 7a, b), respectively. This further reinforces the significant role of fluids in influencing seismicity at these depths, consistent with findings in other seismotectonic regions (Li et al. 2019, 2021; Zhang et al. 2024; Zhou et al. 2025; Aizawa et al. 2017, 2021; Boonchaisuk et al. 2017; Cheng et al. 2022; Ichihara et al. 2023; Borah et al. 2023; Kothyari et al. 2023; Usui et al. 2021, 2024; Cai et al. 2017; Kang et al. 2023; Ogawa et al. 2001, 2002, 2014; Kumar et al. 2017; Umeda et al. 2011; Nagar et al. 2021; Becken and Ritter 2012; Tank et al. 2005; Kaya et al. 2013).

4.3 *Ductile lower crust (> ~ 15 km) and the brittle–ductile transition (BDT)*

Based on Noisagool et al. (2014), the Moho beneath this region is located at a depth of approximately 32 km. The resistivity model of the lower crust, extending from below 15 km (Figs. 6f, g, 7a, b) to the Moho, is characterized by a relatively homogeneous zone of low-to-moderate resistivity. This lower resistivity in the lower crust contrasts with the higher resistivity observed in the upper (Fig. 6b, c) and mid-crustal (Fig. 6d, e) layers, which are associated with the dominance of granite batholiths. As stated in the earlier section, the low resistivity anomalies (approximately 10 Ω m or less in Fig. 6f, g) spread across a larger region and appear horizontally and vertically connected (also see Fig. 4c for wider area). These low resistivity anomalies in the lower crust are potentially indicative of ductile behavior, consistent with observations in other lower crustal environments (Heinson et al. 2018; Li et al. 2019; Cheng et al. 2022; Kothyari et al. 2023; Usui et al. 2021, 2024; Zhou et al. 2025; Zhang et al. 2024).

Their locations are also in closer proximity to the seismogenic region above with a clear connection to the ML and WN conductors (Fig. 6d, e) observed in the mid-crustal layers, as depicted in profile A–A' (Fig. 7a) and C–C' (Fig. 7c) for ML, and profile B–B' (Fig. 7b) and C–C' (Fig. 7c) for WN. With this strong connection, we have, therefore, named them according to their locations as ML_{LC} and WN_{LC} (Figs. 6f, g, 7a–c), suggesting them as present deep fluid sources serving the ML and WN, conductors in the mid-crustal layers.

This significant transition in resistivity at around 15 km depth (Fig. 6d–g) suggests a fundamental change in the physical state of the crust, likely marking the approximate brittle–ductile transition (BDT). This interpretation is supported by the concentration of earthquake hypocenters within the upper and intermediate depths, where brittle deformation is expected to be the dominant mechanism (Figs. 6b–e, 7). Furthermore, this inferred BDT depth, derived from the distinct change in resistivity at 15 km, can also help constrain earlier geological studies (Morley et al. 2011) which estimated it, based on the geothermal gradient, to be around 12–15 km depth.

4.4 The role of the conductors in fluid-driven seismicity: insights into the 2014 Mae Lao earthquake

Based on the MT survey in 2015 (Boonchaisuk et al. 2017), we interpreted the ML conductor (Figs. 6d, e, 7a,

c) as a zone of saline fluids concentrated beneath the MLF at depths of 5 km to mid-crust. Due to its spatial coincidence with the mainshock and aftershocks of the 2014 Mae Lao earthquakes, Boonchaisuk et al. (2017) concluded that the 2014 event was a consequence of these fluids. Their explanation was that the tectonic stress exerted from the north on the MLFZ and PYFZ region increased pore fluid pressure within the fault zone, weakening the frictional strength along the MLF. When the accumulated stress exceeded this reduced strength, it triggered the rupture.

Building upon this foundation of Boonchaisuk et al. (2017), our newly more comprehensive and refined resistivity model, derived from the combination of the 2015 and 2024 MT data sets and shown as plane views at various depths (Fig. 6a–f) and in cross-sectional profiles (Fig. 7a, c), offer further insights that strongly supports a mechanism of fluid-driven seismicity for the 2014 Mae Lao earthquakes and its aftershocks.

We propose here the fluid migration pathways from the deep lower crust upwards into the seismogenic zone of upper crust, consistent with observations in other intraplate seismotectonic settings (Ogawa et al. 2014; Umeda et al. 2011; Li et al. 2019, 2021; Nagar et al. 2021; Usui et al. 2021; Cheng et al. 2022; Zhou et al. 2025; Zhang et al. 2024; Borah et al. 2023; Kumar et al. 2017). Figures 6f and 7a, c indicate the possibility that the ML_{LC} anomaly represents a deeper source region for the fluids, potentially originating from the dehydration of hydrous minerals within the lower crust due to increasing temperature and pressure (e.g., Kothyari et al. 2023; Cheng et al. 2022; Zhang et al. 2024; Borah et al. 2023).

These fluids ascend along these major fault structures and become trapped in the mid-crust, likely due to increasing lithostatic pressure, forming the prominent and overlying ML conductor beneath the MLF (Figs. 6d, e, 7a, c). The interconnected nature of ML_{LC} in the lower crust (Fig. 6f) might allow for a sustained supply of fluids into the mid-crustal ML conductor. The fluids trapped in the ML conductor utilize faults and fractures networks within the brittle upper crust as conduits to further rise to the temporary storage or accumulation in shallower reservoirs, represented by the ML_{north} and ML_{center} conductive anomalies at depths of around 2 km (Figs. 6c, 7a). Interestingly, Fig. 7e suggests a possibility that the fluids from these two spatially separated shallow conductors ascend and coalesce again at even shallower depths, forming the $ML_{shallow}$ conductor (Figs. 6b, 7c) closer to the surface expression of the MLF. The surrounding high resistivity zones (Figs. 6b–e, 7a, c) might act as barriers, further confining and focusing these fluids within the conductive anomalies.

Similar to Boonchaisuk et al. (2017), when the northern tectonic stress is transferred to the region, this results in increased pore fluid pressure within the fault zone at seismogenic depths, thereby decreasing the effective normal stress on the fault (e.g., Umeda et al. 2011; Li et al. 2019; Nagar et al. 2021; Cheng et al. 2022; Zhou et al. 2025; Aizawa et al. 2021; Borah et al. 2023). When the regional tectonic stress exceeded this weakened MLF fault strength, brittle failure and the subsequent mainshock earthquake occurred. The mainshock likely caused an abrupt increase in pore fluid pressure within the surrounding fault zones, potentially contributing to the numerous aftershocks that followed. A direct link between fluid presence and the rupture process is strongly evident by the earthquake hypocenters of both mainshock and aftershocks for the 2014 Mae Lao sequence (Fig. 7a, c) concentrating within or at the edges of these low resistivity zones, a pattern observed in other fluid-driven earthquake settings (Ogawa et al. 2001, 2002, 2014; Umeda et al. 2011; Li et al. 2019; Nagar et al. 2021; Kumar et al. 2017; Aizawa et al. 2017, 2021; Usui et al. 2021, 2024; Zhou et al. 2025; Borah et al. 2023; Cai et al. 2017; Kang et al. 2023).

The compelling evidence for a deep fluid pathway localizing and potentially triggering the 2014 Mae Lao earthquake (Fig. 7a, c) underscores a "unique" mechanism that may be particularly important for understanding intraplate earthquakes. In regions like northern Thailand, where tectonic forces are less direct, fluid–rock interactions can exert a more dominant control on fault behavior compared to the well-established mechanisms at plate boundaries (e.g., Unsworth and Bedrosian 2004; Tank et al. 2005; Kaya et al. 2013; Wannamaker et al. 2014; Becken and Ritter 2012; Egbert et al. 2022; Ichihara et al. 2023).

4.5 Revisiting the 1994 Phan earthquake: sharing the same fluid source as Mae Lao with a distinct fluid pathway

Figure 1b shows that the 1994 Phan earthquake occurred near the Phan Fault (PF), a conjugate structure to the Mae Lao Fault (MLF), where the 2014 earthquake sequence nucleated (Fig. 1c). Interestingly, seismicity in the vicinity of this 1994 Phan earthquake zone (Fig. 1b) has been occurring since 2008, even before the 2014 Mae Lao earthquake. Following the 2014 Mae Lao earthquake (Fig. 1c), the aftershocks overwhelmed the whole region, including this Phan earthquake zone. However, a distinct pattern of small magnitude seismicity can again be observed after 2019 (Fig. 1d), following the relative calm down of the Mae Lao aftershock sequence.

The proximity of the Phan and Mae Lao seismicity regions (Fig. 1b, c), coupled with the shared presence of deep conductive anomalies beneath them (Fig. 7a, c), hints at a common underlying fluid-driven mechanism of the 2014 Mae Lao earthquake and the 1994 Phan earthquake. While both regions appear to share the same deep fluid reservoir within the lower crust (ML_{LC}) migrating to ML in the mid-crust, our 3D resistivity model at shallower depth (Figs. 6c, 7c) reveals a divergence in the fluid ascent pathways from this shared mid-crustal source: one propagating northward towards the 2014 Mae Lao earthquake, and another extending southward towards the 1994 Phan earthquake. This spatial separation in fluid pathways directly explains the distinct spatiotemporal patterns of seismicity observed in the Phan and Mae Lao regions.

In the Mae Lao region (Fig. 7c), fluids ascending from the mid-crustal ML conductor appear to migrate northward and slightly upward towards ML_{north} and then likely continue to rise towards the near-surface conductive zone $ML_{shallow}$ located above. This northerly pathway likely caused the seismicity observed in the Mae Lao sequence. In contrast, another branch of fluids emanating from the same ML conductor appears to track southward and upward towards ML_{south}, subsequently ascending to the southern extent of the near-surface conductive zone $ML_{shallow}$ in the vicinity of the 1994 Phan earthquake hypocenters (Fig. 7c). This distinct southerly pathway likely played a key role in the 1994 Phan earthquakes (Figs. 6c, 7c). This comparative analysis of fluid pathways, inferred from our resistivity model, provides a compelling illustration of how lateral variations in subsurface fluid migration from a common deep source can influence the spatial distribution of intraplate seismicity, even within relatively close proximity.

4.6 Wang Nuea earthquake: mirroring a fluid-driven mechanism of 2014 Mae Lao earthquake

After being a seismically quiet zone for at least a decade (Fig. 1b, c), the occurrence of the unexpected 2019 Ml 4.9 Wang Nuea earthquake (Fig. 1d), approximately 60 km south of the 2014 Mae Lao epicentral region (Fig. 1c), was a significant surprise. It would be understandable to link both of these seismic events despite the 5-year time span between them.

Based on the 2015 and 2024 MT surveys, our resistivity model (Figs. 6, 7b, c) reveals a pre-existing fluid system within the Wang Nuea region, characterized by conductive anomalies from the lower crust (WN_{LC} in Fig. 6f), mid-crust (WN; Fig. 6d, e), and near surface ($WN_{shallow}$; Fig. 6b). These three conductors are clearly displayed in cross sections (Fig. 7a, c), indicating the presence of fluids within and around the Wang Nuea Fault (WNF) and the Wiang Kalong Fault (WKLF). Interestingly, the resistivity model (Fig. 4a) reveals a fluid system (WN_{LC}, WN, and $WN_{shallow}$; Fig. 7b, c) beneath the Wang Nuea region that exhibits a striking similarity in its vertical structure—the presence of lower crustal, mid-crustal, and near-surface conductors—to the fluid system identified beneath the 2014 Mae Lao epicentral region. It is, therefore, readily applicable to employ the same fluid-driven mechanism as for the Mae Lao region to explain the seismicity of the Wang Nuea region.

The inferred fluid pathway initiates from the lower crustal conductor WN_{LC}, which likely serves as the primary source of these fluids. These fluids then ascend and become trapped within the mid-crustal WN conductor before further migrating upwards to the near-surface $WN_{shallow}$ conductor (Fig. 7b, c), likely utilizing the Wang Nuea Fault (WNF) as a conduit. Our resistivity model (Fig. 6f, g) suggests that the lower crustal conductive anomalies represent interconnected fluid networks, ensuring a sustained supply of fluids to both the Wang Nuea and Mae Lao zones. Consistent with the fluid-driven model proposed for the Mae Lao earthquake, the presence of fluids within the WNF likely reduced its frictional strength. This pre-existing fluid-weakened state of the fault likely increased its susceptibility to even minor stress changes originating from the distant 2014 Mae Lao sequence, ultimately triggering the 2019 rupture.

4.7 A unique characteristic of intraplate earthquakes in northern Thailand

The consistent identification of interconnected conductive anomalies, extending from the lower to the upper crust beneath the seismogenic zones of the 1994 Phan, 2014 Mae Lao, and 2019 Wang Nuea earthquakes, as revealed by our MT surveys, represents a notable characteristic of intraplate seismicity in northern Thailand. This recurring pattern strongly indicates that such a multi-tiered fluid system plays a crucial role in weakening fault zones and facilitating their eventual rupture under regional tectonic stress. This interpretation aligns with the prominent role of fluid systems in the genesis of intraplate earthquakes observed in various other regions globally, such as in northwestern India (Kumar et al. 2017; Nagar et al. 2021), western India (Kothyari et al. 2023; Borah et al. 2023), in eastern Tibetan Plateau (Cheng et al. 2022), in northeastern Japan (Usui et al. 2024; Ogawa et al. 2001, 2002, 2014), in central Japan (Usui et al. 2021), in southwest Japan (Umeda et al. 2011), in northern China (Kang et al. 2023), in southwestern China (Cai et al. 2017; Li et al. 2019; Zhou et al. 2025) and in eastern China (Zhang et al. 2024).

This characteristic pattern of shallow, mid-crustal, and deep conductors beneath seismically active regions has potential applications for assessing earthquake hazards in other earthquake-prone areas, particularly in northern Thailand, such as the Mae Tha Fault Zone near Chiang Mai city and the Mae Hong Son Fault Zone in Mae Hong Son. Furthermore, similar assessments could be conducted in western Thailand, including areas around the Three Pagoda Fault Zone and the Sri Sawat Fault Zone in Kanchanaburi, which is the closest such region to Bangkok, the capital of Thailand. These northern and western areas are of particular interest due to the significant impact felt from recent large earthquakes in Mandalay, Myanmar. The detection of this characteristic subsurface conductive signature within fault zones may offer a valuable tool for spatial forecasting of future earthquake locations.

5 Conclusion

Following the Mw 6.3 Mae Lao earthquake in 2014, our initial magnetotelluric (MT) survey identified a mid-crustal conductive anomaly (ML) beneath the Mae Lao Fault (MLF), which we interpreted as a saline-fluid zone that likely weakened the fault and contributed to its rupture (Boonchaisuk et al. 2017). Five years later, the unexpected Ml 4.9 Wang Nuea earthquake occurred in a previously seismically quiet area, approximately 60 km south of the Mae Lao epicentral region, suggesting a potential link between the two events. Our earlier MT survey had also detected a mid-crustal conductor (WN) beneath the Wang Nuea Fault (WNF), initially interpreted as a source for surface hot springs. To further investigate the nature of this WN conductive anomaly, we conducted an additional MT survey in 2024, deploying more stations around the Wang Nuea region.

Our integrated 3D resistivity model, derived from the combined 2015 and 2024 MT data sets, provides a refined image of the subsurface beneath the Mae Lao region following the 2014 earthquake. This model reveals a complex, multi-tiered conductive system characterized by a lower crustal conductor (ML_{LC}), a prominent mid-crustal conductor (ML), a northward extension (ML_{north}), a southward extension (ML_{south}), and a near-surface conductor ($ML_{shallow}$). This detailed structure supports the interpretation of interconnected fluid pathways ascending from a deep source and influencing the seismogenic zone of the Mae Lao Fault (MLF). Given the proximity of the 1994 Phan earthquake (Mw 5.2) to the 2014 Mae Lao earthquake, we investigated earthquake mechanisms for both events. Our 3D resistivity model indicated that both earthquakes shared a deep fluid source linked to ML_{LC} and a mid-crustal source linked to ML. However, diverging from ML upwards, fluids appear to migrate southward to ML_{south} before rising towards the near surface in the vicinity of the Phan earthquake hypocenters, while fluids migrate northward to ML_{north} to ascend towards the surface in the Mae Lao earthquake hypocenters.

In the Wang Nuea region, our integrated MT model confirmed the presence of a well-defined conductive anomaly (WN) beneath the Wang Nuea region, exhibiting a similar multi-tiered structure to that observed beneath Mae Lao, with conductive zones extending from the lower crust (WN_{LC}) to the mid-crust (WN) and near-surface ($WN_{shallow}$). This refined imaging strongly supports the interpretation of a pre-existing fluid system within the Wang Nuea fault zone. The inferred fluid pathway, ascending from WN_{LC} and accumulating in WN before rising to $WN_{shallow}$ along the WNF, mirrors the fluid-driven mechanism proposed for the Mae Lao earthquake, suggesting that a similar weakening of the WNF by crustal fluids likely contributed to the 2019 rupture, possibly triggered by subtle stress transfer from the earlier Mae Lao event.

The consistent presence of such multi-tiered conductive systems associated with the 1994 Phan, 2014 Mae Lao, and 2019 Wang Nuea earthquakes indicates a potential characteristic of intraplate seismogenesis within this region of northern Thailand. The identification of this subsurface conductive signature from the magnetotelluric surveys across multiple events offers a valuable geophysical marker for assessing seismic hazards and potentially spatial forecasting of future earthquake locations in other tectonically similar areas of northern Thailand.

Abbreviations

MT	Magnetotelluric
TMD	Thailand Meteorological Department
MCFZ	Mae Chan Fault Zone
PYFZ	Phayao Fault Zone
DMR	Department of Mineral Resources
MKF	Mae Korn Fault
MLF	Mae Lao Fault
MSF	Mae Suai Fault
PF	Phan Fault
WNF	Wang Nuea Fault
WKLF	Wiang Kalong Fault
DKMSF	Doi Khun Mae Suk Fault
PYF	Phayao Fault
USGS	United States Geological Survey
FB	Fang Basin
MSB	Mae Suai Basin
CRB	Chiang Rai Basin
CRPB	Chiang Rai–Phayao Basin

Acknowledgements

This research has been supported by the Thailand Center of Excellence in Physics (ThEP).

Author contributions

PA conducted the field surveys, performed the data analysis, contributed to the discussion of the results, took a lead role in writing the manuscript, and prepared all the figures. WS served as the primary investigator for this research, contributed significantly to the data analysis and discussion of the findings, and played a key role in writing the manuscript. SB and PN provided

valuable assistance with the field surveys and contributed to some aspects of the data analysis. YO assisted in conceptualization and discussion.

Funding
Open access funding provided by Mahidol University. Funding was provided by Thailand Center of Excellence in Physics (ThEP-61-PHM-MU1 and ThEP-68-ThEP-MU).

Availability of data and materials
Field data can be provided by contacting the corresponding author.

Declarations

Ethics approval and consent to participate
Not applicable.

Consent for publication
Not applicable.

Competing interests
The authors do not have any potential competing interests.

Author details
[1]Department of Physics, Faculty of Science, Mahidol University, 272 Rama 6 Road, Rachatawee, Bangkok, Thailand. [2]ThEP Center, Commission On Higher Education, 328, Si Ayutthaya Road, Rachatawee, Bangkok, Thailand. [3]Geoscience Program, Mahidol University, Kanchanaburi Campus, Saiyok, Kanchanaburi, Thailand. [4]Multidisciplinary Resilience Research Center, Institute of Science Tokyo, Tokyo 152-8551, Japan. [5]Research Center for Prediction of Earthquakes and Volcanic Eruptions, Tohoku University, Sendai 980-8578, Japan.

Received: 4 May 2025 Accepted: 23 September 2025
Published online: 24 October 2025

References

Aizawa K et al (2017) Seismicity controlled by resistivity structure: the 2016 Kumamoto earthquakes, Kyushu Island. Jpn Earth Planets Space 69:4. https://doi.org/10.1186/s40623-016-0590-2
Aizawa K, Takakura S, Asaue H, Koike K, Yoshimura R, Yamazaki KI et al (2021) Electrical conductive fluid-rich zones and their influence on the earthquake initiation, growth, and arrest processes: observations from the 2016 Kumamoto earthquake sequence, Kyushu Island, Japan. Earth Planets Space 73:1–12. https://doi.org/10.1186/s40623-020-01340-w
Amatyakul P, Rung-Arunwan T, Siripunvaraporn W (2015) A pilot magnetotelluric survey for geothermal exploration in Mae Chan region, northern Thailand. Geothermics 55:31–38
Amatyakul P, Boonchaisuk S, Rung-Arunwan T, Vachiratienchai C, Wood SH, Pararai K, Fuangswasdi A, Siripunvaraporn W (2016) Exploring the shallow geothermal fluid reservoir of Fang geothermal system, Thailand via a 3-D magnetotelluric survey. Geothermics 64:516–526
Amatyakul P, Wood SH, Rung-arunwan T, Vachiratienchai C, Prommakorn N, Chanapiwat P, Siripunvaraporn W (2021) An assessment of a shallow geothermal reservoir of Mae Chan hot spring, northern Thailand via magnetotelluric surveys. Geothermics 95:102137. https://doi.org/10.1016/j.geothermics.2021.102137
Amatyakul P, Siripunvaraporn W, Rung-Arunwan T, Vachiratienchai C, Pirarai K, Prommakorn N (2023) A decade of successful magnetotelluric surveys for delineating shallow geothermal reservoirs beneath nonvolcanic hot springs in Thailand. Geophysics 88(5):WB55–WB69. https://doi.org/10.1190/geo2022-0486.1
Becken M, Ritter O (2012) Magnetotelluric studies at the San Andreas fault zone: implications for the role of fluids. Surv Geophys 33:65–105
Boonchaisuk S, Siripunvaraporn W, Ogawa Y (2013) Evidence for middle Triassic to Miocene dual subduction zones beneath the Shan-Thai terrane, western Thailand from magnetotelluric data. Gondwana Res 23(4):1607–1616. https://doi.org/10.1016/j.gr.2012.08.009
Boonchaisuk S, Noisagool S, Amatyakul P, Rung-Arunwan T, Vachiratienchai C, Siripunvaraporn W (2017) 3-D magnetotelluric imaging of the Phayao Fault Zone, Northern Thailand: evidence for saline fluid in the source region of the 2014 Chiang Rai earthquake. J Asian Earth Sci 147:210–221
Borah UK, Patro PK, Raju K, Reddy KC, Babu N, Rao PR, Rao NP (2023) Role of fluid on seismicity of an intra-plate earthquake zone in Western India: an electrical fingerprint from magnetotelluric study. Earth Planets Space 75(1):149
Cai J, Chen X, Xu X, Tang J, Wang L, Guo C, Han B, Dong Z (2017) Rupture mechanism and seismotectonics of the Ms6.5 Ludian earthquake inferred from three-dimensional magnetotelluric imaging. Geophys Res Lett 44:1275–1285. https://doi.org/10.1002/2016GL071855
Charusiri P, Pum-Im S (2009) Cenozoic tectonic evolution of major sedimentary basins in Central, Northern, and the Gulf of Thailand. Bull Earth Sci Technol 2:40–62
Charusiri P, Clark AH, Farrad E, Archibald D, Charusiri B (1993) Granite belts in Thailand: evidence from the 40Ar/39Ar geochronological and geological syntheses. J Southeast Asian Earth Sci 8:127–136
Cheng Y, Kong Y, Wang Z, Huang Y, Hu X (2022) Crustal electrical structure of the Ganzi Fault on the Eastern Tibetan Plateau: implications for the role of fluids in earthquakes. Remote Sens 14:2990. https://doi.org/10.3390/rs14132990
Department of Mineral Resource (2023) Active faults in Thailand. Department of Mineral Resource, Thailand (**in Thai**)
Egbert GD (1997) Robust multiple-station magnetotelluric data processing. Geophys J Int 130:475–496
Egbert GD, Yang B, Bedrosian PA, Key K, Livelybrooks DW, Schultz A, Kelbert A, Parris B (2022) Fluid transport and storage in the Cascadia forearc influenced by overriding plate lithology. Nat Geosci 15(8):677–682. https://doi.org/10.1038/s41561-022-00981-8
Heinson G, Soeffky P, Thiel S, Didana Y, Robertson K (2018) Electrical resistivity maps of the Australian Lower Crust. ASEG Ext Abstr 2018(1):1–5. https://doi.org/10.1071/ASEG2018abP039
Ichihara H, Kasaya T, Baba K et al (2023) 2D resistivity model around the rupture area of the 2011 Tohoku-oki earthquake (*M*w 9.0). Earth Planets Space 75:82. https://doi.org/10.1186/s40623-023-01828-1
Kang M, Huang Y, Xin H, Song J, Zhang X, Peng R (2023) Crustal structures and seismogenic setting of the West Henan Region, North China, as revealed by magnetotelluric imaging. Pure Appl Geophys 180(11):3835–3853
Kanthiya S, Mangkhemthong N, Morley CK (2019) Structural interpretation of Mae Suai Basin, Chiang Rai Province, based on gravity data analysis and modelling. Heliyon. https://doi.org/10.1016/j.heliyon.2019.e01232
Kaya T, Kasaya T, Tank SB, Ogawa Y, Tuncer MK, Oshiman N, Honkura Y, Matsushima M (2013) Electrical characterization of the North Anatolian Fault Zone underneath the Marmara Sea, Turkey by ocean bottom magnetotellurics. Geophys J Int 193:664–677
Kothyari GC, Dumka RK, Chopra S, Singh KD, Tamta BK, Kamra C (2023) Triggering mechanism and brittle-ductile dynamics of active faults in the south-central Saurashtra horst, Gujarat, western India: a geospatial, geological, and geophysical approach. J Asian Earth Sci X 9:100155
Kumar GP, MaheshNagar P, Mahender M, Kumar E, Mohan V, Kumar K (2017) Role of deep crustal fluids in the genesis of intraplate earthquakes in the Kachchh region, northwestern India. Geophys Res Lett. https://doi.org/10.1002/2017GL072936
Li X, Bai D, Ma X, Chen Y, Varentsov IM, Xue G, Xue S, Lozovsky I (2019) Electrical resistivity structure of the Xiaojiang strike-slip fault system (SW China) and its tectonic implications. J Asian Earth Sci 176:57–67
Li D, Yu N, Li X, Wang E, Li R, Wang X (2021) Magnetotelluric evidence of fluid-related seismicity beneath the Chuxiong Basin, SE Tibetan Plateau. Tectonophysics 816:229039
Lukkunaprasit P, Ruangrassamee A, Boonyatee T, Chintanapakdee C, Jankaew K, Thanasisathit N, Chandrangsu T (2015) Performance of structures in the M_w 6.1 Mae Lao earthquake in Thailand on May 5, 2014 and implications for future construction. J Earthq Eng 20(2):219–242. https://doi.org/10.1080/13632469.2015.1051636
Manopkawee P, Mankhemthong N, Wiwegwin W, Kanthata S (2025) Spatial landscape response to active tectonics along the Western Mae Chan Fault, Northern Thailand. J Asian Earth Sci 278

Metcalfe I (2013) Gondwana dispersion and Asian accretion: tectonic and palaeogeographic evolution of eastern Tethys. J Asian Earth Sci 66:1–33
Metcalfe I (1997) The Palaeo-Tethys and Palaeozoic-Mesozoic tectonic evolution of Southeast Asia. In: Proceedings of the international conference on stratigraphy and tectonic evolution of Southeastern Asia and the South Pacific (GEOTHAI '97). Department of Mineral Resources, Thailand, pp 260–272
Morley CK, Charusiri P, Watkinson IM (2011) Structural geology of Thailand during the Cenozoic. In: Ridd MF, Barber AJ, Crow MJ (eds) The geology of Thailand. Geological Society of London, New York, pp 273–334
Nagar M, Pavankumar G, Mahesh P, Rakesh N, Chouhan AK, Nagarjuna D, Chopra S, Kumar MR (2021) Magnetotelluric evidence for trapped fluids beneath the seismogenic zone of the Mw6.0 Anjar earthquake, Kachchh intraplate region, Northwest India. Tectonophysics 814:228969
Noisagool S, Boonchaisuk S, Pornsopin P, Siripunvaraporn W (2014) Thailand's crustal properties from tele-seismic receiver function studies. Tectonophysics 632:64–75
Noisagool S, Boonchaisuk S, Pronsopin P, Siripunvaraporn W (2016) The regional moment tensor of the 5 may 2014 Chiang Rai earthquake (Mw = 6.5), northern Thailand, with its aftershocks and its implication to the stress and the instability of the Phayao Fault Zone. J Asian Earth Sci 127:231–246
Ogawa Y, Mishina M, Goto T, Satoh H, Oshiman N, Kasaya T, Takahashi Y, Nisitani T, Sakanaka S, Uyeshima M, Takahashi Y, Honkura Y, Matsushima M (2001) Magnetotelluric imaging of fluids in intraplate earthquakes zones, NE Japan back arc. Geophys Res Lett 28:3741–3744
Ogawa Y, Takakura S, Honkura Y (2002) Resistivity structure across Itoigawa-Shizuoka tectonic line and its implications for concentrated deformation. Earth Planets Space 54:1115–1120
Ogawa Y, Ichiki M, Kanda W, Mishina M, Asamori K (2014) Three-dimensional magnetotelluric imaging of crustal fluids and seismicity around Naruko volcano, NE Japan. Earth Planets Space 66:1–13
Pananont P et al (2017) Seismotectonics of the 2014 Chiang Rai, Thailand, earthquake sequence. J Geophys Res Solid Earth 122:6367–6388. https://doi.org/10.1002/2017JB014085
Siripunvaraporn W (2012) Three-dimensional magnetotelluric inversion: an introductory guide for developers and users. Surv Geophys 33(1):5–27. https://doi.org/10.1007/s10712-011-9122-6
Siripunvaraporn W, Egbert G (2009) WSINV3DMT: vertical magnetic field transfer function inversion and parallel implementation. Phys Earth Planet Inter 173:317–329
Siripunvaraporn W, Sarakorn W (2011) An efficient data space conjugate gradient Occam's method for three-dimensional magnetotelluric inversion. Geophys J Int 186(2):567–579. https://doi.org/10.1111/j.1365-246X.2011.05079.x
Siripunvaraporn W, Egbert G, Lenbury Y (2002) Numerical accuracy of magnetotelluric modeling: a comparison of finite difference approximations. Earth Planets Space 54:721–725
Siripunvaraporn W, Egbert G, Lenbury Y, Uyeshima M (2005) Three-dimensional magnetotelluric inversion: data-space method. Phys Earth Planet Inter 150:3–14
Socquet A, Simons W, Vigny C, McCaffrey R, Subarya C, Sarsito D et al (2006) Microblock rotations and fault coupling in SE Asia triple junction (Sulawesi, Indonesia) from GPS and earthquake slip vector data. J Geophys Res Solid Earth 111:1–15. https://doi.org/10.1029/2005JB003963
Sone M, Metcalfe I (2008) Parallel tetyan sutures in mainland Southeast Asia: new insights for Palaeo-Tethys closure and implications for the Indosinian Orogeny. C R Geosci 340:166–179
Sone M, Metcalfe I, Chaodumrong P (2012) The Chanthaburi terrane of southeastern Thailand: stratigraphic confirmation as a disrupted segment of the Sukhothai arc. J Asian Earth Sci 61:16–32
Tadapansawut T, Yagi Y, Okuwaki R et al (2022) Complex rupture process on the conjugate fault system of the 2014 Mw 6.2 Thailand earthquake. Prog Earth Planet Sci 9:26. https://doi.org/10.1186/s40645-022-00484-5
Tank SB, Honkura Y, Ogawa Y, Matsushima M, Oshiman N, Tuncer MK, Celik C, Tolak E, Isikara AM (2005) Magnetotelluric imaging of the fault rupture area of the 1999 Izmit (Turkey) earthquake. Phys Earth Planet Inter 150:213–225
Thongyoy W, Siripunvaraporn W, Amatayakul P, Rung-Arunwan T, Baba K (2025) An efficient decoupled 3-D axial anisotropic resistivity inversion for magnetotelluric data with OpenMP parallelization. Earth Planets Space 77(1):7
Tsutsumi H, Sato T (2009) Tectonic geomorphology of the southernmost sagaing fault and surface rupture associated with the May 1930 Pegu (Bago) Earthquake, Myanmar. Bull Seismol Soc Am 99(4):2155–2168. https://doi.org/10.1785/0120080113
Umeda K, Asamori K, Negi T, Kusano T (2011) A large intraplate earthquake triggered by latent magmatism. J Geophys Res. https://doi.org/10.1029/2010JB007963
Unsworth MJ, Bedrosian PA (2004) Electrical resistivity structure at the SAFOD site from magnetotelluric exploration. Geophys Res Lett 31:L12S05
Usui Y, Uyeshima M, Ogawa T, Yoshimura R, Oshiman N, Yamaguchi S et al (2021) Electrical resistivity structure around the Atotsugawa fault, central Japan, revealed by a new 2-D inversion method combining wideband-MT and network-MT data sets. J Geophys Res Solid Earth 126:e2020JB020904. https://doi.org/10.1029/2020JB020904
Usui Y, Uyeshima M, Hase H, Ichihara H, Aizawa K, Koyama T et al (2024) Three-dimensional electrical resistivity structure beneath a strain concentration area in the back-arc side of the northeastern Japan arc. J Geophys Res Solid Earth 129:e2023JB028522. https://doi.org/10.1029/2023JB028522
Uttamo W, Elders C, Nichols G (2003) Relationships between Cenozoic strike-slip faulting and basin opening in northern Thailand. Geol Soc Spec Publ 210:89–108
Wannamaker PE, Evans RL, Bedrosian PA, Unsworth MJ, Maris V, McGary RS (2014) Segmentation of plate coupling, fate of subduction fluids, and modes of arc magmatism in Cascadia, inferred from magnetotelluric resistivity. Geochem Geophys Geosyst 15:4230–4253
Zhang Y, Jin S, Ye G, Zhang H, Wei W, Dong H, Gao J (2024) Intraplate seismic mechanisms in the Zhangjiakou-Bohai seismic belt: insights from magnetotelluric data. Earth Planets Space 76(1):174
Zhou Z, Yu N, Wang T, Kong W, Chen H, Li T (2025) Episodic earthquakes controlled by the migration of crustal fluids and fault valve behavior. Geophys Res Lett 52:e2024GL114093. https://doi.org/10.1029/2024GL114093

Publisher's Note